A Hierarchical Predictive Control Approach for Wireless Electric Vehicle Energy Network with Integrated Microgrids Incorporating Degradation Costs

Ye Duan, *Student Member*, *IEEE*, Kwok Tong Chau, *Fellow*, *IEEE*, Wei Liu, *Senior Member*, *IEEE*, and Yunhe Hou, *Senior Member*, *IEEE*

***Abstract*—Integrating wireless electric vehicle energy network with microgrids benefits vehicle owners and grid operators. Yet, economical and reliable operations for such combinations under renewable energy uncertainties remain examined. To address this, achieving cost-effective and reliable performance, a novel hierarchical predictive control approach is utilized. Its core innovation schedules optimal power dispatches for integrated microgrids using different time frames with upper-level control minimizing energy costs and battery energy storage systems' degradation costs, whereas lower-level control additionally lowers degradation costs. Moreover, the approach inherently enhances system reliability by minimizing power fluctuations using control references from upper-level control and state variables feedback from lower-level control under renewable energy uncertainties. The unique cross-time-frame integration of this approach enables modeling and incorporating degradation costs to adapt costs associated with longer time frames into optimal power dispatches in shorter time frames, reflecting the unique features of hybrid energy storage systems. Comparative studies reveal that various energy storage systems can be employed at different hierarchical control levels for tailored power distribution objectives. Effectiveness of the utilized approach is confirmed by comparing it with control benchmarks through its average reduction of energy costs by 348$, degradation costs by 10.03$, and expected energy not served down to 0 Wh/quarter.**

***Index Terms*--Wireless electric vehicle energy network, energy informatics, renewable energy, wireless charging, degradation.**

I. Introduction

TRANSPORTATION electrification is becoming a significant goal in modern society, which facilitates the increasing adoption of electric vehicles (EVs). Considering the interaction between the transportation network and the power grid, the Vehicular Energy Network (VEN) has been reported, where EVs travel through an electrified road network with (dis)charging and storage facilities. Each junction may also have an energy supply, such as nearby renewable energy sources (RES) [1].

With the rapid development of wireless power transfer(WPT) technologies, it has been recognized for its convenience, safety, and flexibility. Thus, academia and industry have regarded WPT as a promising solution for charging EVs by deploying wireless charging pads beneath the road to form dynamic wireless charging (DWC) lanes. More precisely, EVs can charge on DWC lanes to extend range and reduce range anxiety. They receive shallow, frequent chargings rather than deep, infrequent ones, which can reduce battery size and prolong battery life. Last but not least, wired charging requires dedicated, costly urban space, but DWC avoids that and shortens wait times during rush hours [2].

With these benefits, DWC can be integrated with transportation and electricity networks [3]-[6]. However, implementing long-distance DWC lanes across road networks on a large scale is costly. A more cost-effective approach is to designate short-distance DWC lanes at specific locations with suitable traffic capacity, this forms the wireless EV energy network (WEVEN) consisting of DWC infrastructures with DWC lanes. In this context, various research has been conducted. A novel method was investigated to solve the multisource–multidestination energy routing problem for a WEVEN, minimizing the system energy loss while satisfying the capacity constraints of vehicular paths [7]. Besides, a prototype was explored for wireless energy trading in the WEVEN [8].

As human society is working towards a sustainable future with an increasing need to promote economical operations by reducing energy costs. RES can tackle these challenges by transitioning the energy supply from fossil fuels to renewable energy. However, due to RES uncertainties, including generation fluctuations, intermittency and forecast errors (FEs), microgrids are used to resolve these issues [9]. Additionally, if WEVEN is directly connected to the main grid, the charging demand of large-scale WEVEN may place significant pressure on the main grid's operations, which may lead to congested feeders, overloaded components, and excessive faults. Similarly, microgrids can serve as a solution to mitigate the charging impact of large-scale WEVEN on the main grid [10].

This work was supported in part by the Hong Kong Research Grants Council, Hong Kong Special Administrative Region, China, under Grant T23-701/20-R and Grant 17206222, and in part by The Hong Kong Polytechnic University under Grant P0048560 and P0046563. (*Corresponding author: Kwok Tong Chau*)

Y. Duan and Y. Hou are with the Department of Electrical and Electronic Engineering, The University of Hong Kong, Hong Kong, China (e-mail: duanye@connect.hku.hk; yhhou@eee.hku.hk).

K.T. Chau and W. Liu are with the Research Centre for Electric Vehicles and Department of Electrical and Electronic Engineering, The Hong Kong Polytechnic University, Hong Kong, China (e-mail: k.t.chau@polyu.edu.hk; wei.liu@polyu.edu.hk).

Accordingly, considering the aspects above, as much electricity as possible supplied to the WEVEN should be low-carbon electricity produced by RES in microgrids to reduce dependence on electricity from the main grid. Consequently, to handle the above energy challenges in the future urban scenario, the combination of WEVEN and microgrids, which is the DWC infrastructure as the load in integrated microgrids, shall be examined.

In addition, the RES uncertainties can cause system robustness issues since RES energy might be unavailable during adverse weather conditions when electricity is needed, and energy storage systems (ESS) are typically integrated into microgrids to offset these power mismatches. To meet varying operational requirements, hybrid ESS (HESS) is utilized, with ESS possessing large energy densities, such as the battery energy storage systems (BESS) managing excess energy exchange, while ESS with high power ratings addresses instant power mismatches. Furthermore, in the economical operation of the WEVEN with integrated microgrids, not only energy costs but also BESS degradation costs should be considered, since real-time operations of BESS, which involve frequent (dis)charging, can significantly affect its long-term lifespan. Thus, the battery's life would considerably deteriorate, necessitating the accurate reflection of long-term BESS degradation costs in real-time power dispatches for the WEVEN with integrated microgrids [11]. Resultantly, different time frames are necessary for the comprehensive design of control approaches when dealing with the degradation costs of HESS. Finally, and importantly, RES uncertainties can cause power fluctuations, which may contribute to potential reliability issues as reflected by expected energy not served (EENS) during microgrid operations [12], [13]. Thereby, it also ought to be studied to guarantee the highly reliable operation of the WEVEN with integrated microgrids.

Currently, there is some research on the combination of DWC and microgrids. A collaborative predictive control strategy was presented to allocate charging power to individual DWC EVs in the microgrid and alleviate its charging impacts on the main grid, while accounting for the charging needs of different DWC EVs [14]. A novel microgrid structure involving DWC EVs as distributed energy storage was introduced to regulate energy and stabilize renewable generation, with a bi-level framework for microgrid capacity planning through maximizing utility and minimizing social costs [15]. [16] discusses the optimal deployment of DWC lanes with microgrid integration profitably overcomes EV range anxiety, validated via traffic and grid simulations. [17] integrates DWC with a microgrid, using particle swarm optimization-optimized energy management in both island and grid-connected modes to enhance stability via load-supply balance and maximize cost efficiency. The Improved Harris Hawk Optimization algorithm minimizes operational costs and enhances efficiency for wireless EV charging stations within a hybrid renewable microgrid, outperforming benchmarks while ensuring resilience against renewable intermittency is studied in [18]. A game-theoretic framework synergizes DWC traffic and microgrid scheduling via best-response optimization to balance economics and emissions, is proposed in [19]. [20] introduces a game-driven microgrid network that optimizes wireless charging infrastructure via connected EVs coordination for grid stability and profits. [21] proposes a Simulink-optimized standalone microgrid with renewables and storage powers highway wireless EV charging for sustainable transportation. An enhanced microgrid dispatch stabilizes the DWC of EVs during grid transients is studied in [22]. However, the aforementioned research does not address the connection between the WEVEN and microgrids. Also, [14]-[18] and [20]-[22] fail to consider BESS degradation costs, which are highly associated with economical operations. Moreover, [21] [22] neglect reliable operations, while [16] [19] [21] ignore RES uncertainties.

Because current DWC and microgrids combined research merely considers both economical and reliable operations under RES uncertainties. A hierarchical predictive control approach for the WEVEN with integrated microgrids is utilized to fill these research gaps in this paper, and it is superior in the following perspectives compared with the collaborative predictive control [14] and optimal control [23] benchmarks, with the following contributions:

1) Using the longer time frame in the upper-level control, the maximum possible amount of electricity supplied to the WEVEN comes from RES in integrated microgrids, lowering energy costs and ensuring more economical operations.

2) BESS degradation costs are reduced through the longer time frame in the upper-level control and the shorter time frame in the lower-level control, thus also contributing to the more economical operation.

3) The WEVEN with integrated microgrids operates more reliably by optimizing EENS through minimizing power fluctuations utilizing control references from upper-level controls and state variables feedback from lower-level controls.

The summarized novelty of the utilized approach is the incorporation of those merely considered aspects stated above while simultaneously achieving better economical and reliable performance for the WEVEN with integrated microgrids, by leveraging different time frames in the upper and lower control levels under various RES uncertainties. The remainder of this paper is arranged as follows. Section II proposes the WEVEN modeling that contains the analysis of DWC infrastructures along with the transportation network and flow models involved. Section III presents the structure, RES uncertainties' modeling, and degradation cost formulation for integrated microgrids. The utilized approach is detailed in Section IV. Section V illustrates the comparative case evaluations to verify the effectiveness and robustness of the utilized approach. Section VI draws the conclusion.

II. Wireless Electric Vehicle Energy Network Modeling

A. Structure of WEVEN with Integrated Microgrids

The WEVEN, which is modeled based on the link-based transportation network model [24], consists of several DWC infrastructures, each containing DWC lanes in two ways with

the integrated microgrid, which can exchange power with the main grid if necessary. The complete figure showing the WEVEN with integrated microgrids connected to the main grid is shown in Fig. 1. EVs traverse on the DWC lanes, so the power demand for DWC EVs is dictated by the traffic volume, meaning that the hourly vehicular flow changes over time. Accordingly, the hourly total power demanded by DWC EVs is time-varying, and it is related to the hourly total number of DWC EVs traveling on DWC lanes within the individual DWC infrastructure of the WEVEN.

B. Dynamic Wireless Charging Infrastructure Analysis

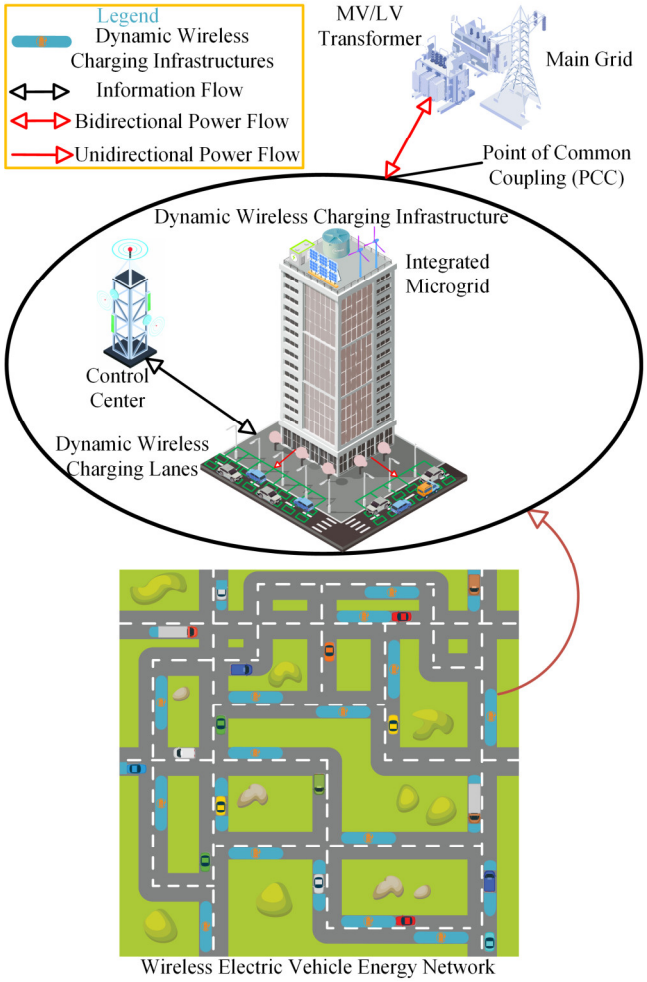

Fig. 1. WEVEN with integrated microgrids connected to main grid.

We assume that DWC EVs move continuously on DWC lanes, similar to water flowing through pipes. In other words, we ignore the discrete nature of vehicles arriving at and departing from DWC lanes [7]. That is rather than tracking each DWC electric vehicle in the WEVEN, this assumption enables us to monitor the overall network flow of DWC EVs through the time-dependent link-loading transportation flow model [24], as modeling the charging of individual DWC EVs is beyond the scope of this research. To clarify more on this assumption, it allows us to solve the problem with reduced complexity according to network flow theories. In the link-based transportation network model, each link represents a direct connection between two nodes for transporting commodities. This is illustrated by modeling a road network as a graph: nodes correspond to junctions, links represent roads, and the commodity flowing on these links is quantified as vehicles per unit time, which is $N(t)$, defined as the vehicular flow of DWC EVs for the DWC infrastructure on each link in this time-variant WEVEN [7] [25]. Also, this study adopts the research scenario of Hong Kong, and this assumption is especially suitable for cities with high traffic volumes. Since Hong Kong has an annual average daily traffic (AADT) of more than 11000 vehicles [26], and conventionally, the high traffic volume is defined as the AADT being above 10000 vehicles [27]. With this assumption, energy can be charged to DWC EVs continuously in the DWC infrastructure concerning time in hours, and the hourly total power transmitted to DWC EVs from DWC lanes within a DWC infrastructure is:

$$P_{DWCEVs}(t) = \frac{N(t)\alpha_{EV}\alpha_{DWCEV}kP_{DWC}L}{Vt} \quad (1)$$

where k is seasonal scaling factors related to the hourly total number of DWC EVs traversing on DWC lanes within the individual DWC infrastructure of the WEVEN since the vehicle traveling pattern varies with seasons; α_{EV} denotes the percentage of EVs among all registered motor vehicles; α_{DWCEV} represents the percentage of DWC EVs within all EVs; P_{DWC} is the DWC rate of DWC lanes; L is the length of DWC lanes and V is the average velocity of the DWC EVs passing through DWC lanes, as they are crucial factors in modeling EV wireless charging demand, which is different from traditional wired charging; and t is the time of interest.

III. Integrated Microgrid Modeling

A. Integrated Microgrid Structure

The structural diagram of the DWC infrastructure integrated microgrid is illustrated in Fig. 2. Without limiting the generality, the integrated microgrid comprises the RES of wind and solar power generation systems, a HESS of BESS and flywheel energy storage systems (FESS), the aggregated charging load of DWC EVs, and the point of common coupling connected to the main grid. In practice, the microgrid can function either connected to the main grid or independently as an islanded grid based on system needs, RES generation and energy market situations. Unless stated otherwise, this paper will focus on the grid-connected mode.

B. Renewable Power Production

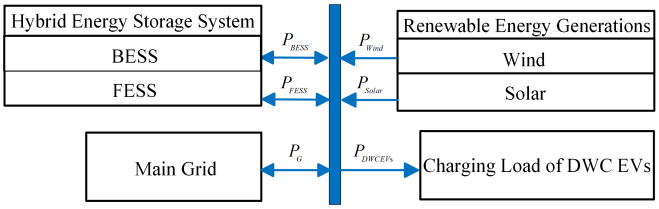

Fig. 2. System model of integrated microgrid.

Implementing RES in the microgrid makes monitoring the real-time balance between supply and demand more challenging. The integrated microgrid is designed with two RES systems: wind turbines and solar panels. The solar power

generated from solar RES, $P_{Solar}(t)$, is modeled using [28]:

$$P_{Solar}(t)=\eta_{Solar}C_{Solar}G(t) \quad (2)$$

where η_{Solar} is the operation efficiency of solar panels, C_{Solar} symbolizes the installed capacity of solar panels in integrated microgrids, and $G(t)$ indicates the solar radiation intensity at time t, respectively. The solar radiation intensity can be calculated based on the hourly total all-sky surface photosynthetically active radiation, $PAR(t)$ [29]:

$$G(t)=2PAR(t) \quad (3)$$

While the wind power produced by wind RES is [30]:

$$P_{Wind}(t)=0.5C_P\rho_{Air}A_{WT}V_{WT}(t) \quad (4)$$

where C_p and A_{WT} stand for the coefficient of performance and the rotor blades swept area of wind turbines in integrated microgrids. ρ_{Air} and $V_{WT}(t)$ designate the air's density and the wind speed at time t around the wind turbines. Because solar radiation intensity and wind speed fluctuate each season, the integrated microgrid's exact solar and wind power generations differ in the four seasons.

Also, solar power generation exhibits significant variation due to passing clouds, while wind power generation is closely tied to wind speed. These factors contribute to the RES outputs' uncertainties of FEs, generation fluctuations, and intermittency [31] within the integrated microgrid. Since generation fluctuations and intermittency are already reflected in the real-world weather-related data used in this study, RES uncertainties are also modeled through discrete Gaussian distributed random variables-based FEs [32], which further tests the robustness of the utilized approach. Generally, FEs for solar power can reach 25%, while wind power FEs average over 10%, depending on the various irradiance and wind speed forecasting methods [33].

C. Energy Storage System Integration and Degradation Cost

The design characteristics of the HESS differ based on energy density, power density, cost, and lifespan. Typically, the preferred design configuration for the microgrid is a hybrid of ESS, where one ESS offers high energy densities and the other has a high power density [34]. Ergo, in this paper, the HESS in integrated microgrids consists of the BESS and FESS due to their complementary features. The BESS can hold a substantial amount of electrical energy because of its high energy density, whereas the FESS provides rapid (dis)charging responses with its high power density [35]. The primary roles of HESS involve balancing the instantaneous power imbalances while maintaining the economical and reliable operation of the entire WEVEN with integrated microgrids. Therefore, the BESS and FESS ought to have distinct objectives, the former is mainly tasked with functioning as the distributed generation unit to lower energy costs, whereas the latter should address immediate power discrepancies to reduce BESS degradation cost and minimize power fluctuations to enhance reliable operations. Our hierarchical time-scale design is essential for optimal HESS operations. The upper-level's longer horizon minimizes energy costs and BESS degradation costs through strategic energy management, while the lower-level's shorter time frame deploys FESS to absorb power transients to further optimize degradation costs and enhance the system's reliability. This separation allows the BESS to focus on cost-effective energy scheduling, while the FESS provides instantaneous stabilization—enhancing system reliability and extending BESS lifespan.

Assessing the BESS degradation is crucial for evaluating the economical operation of the microgrid analytically [36]. To precisely model the cost characteristics for the WEVEN with integrated microgrids, the BESS degradation cost is examined and formulated mathematically. As for the FESS, it can endure thousands of deep cycles, far surpassing the BESS, demonstrating a significantly extended lifespan over the long term. Also, the FESS is not constrained by cycling stress with (dis)charging rates that minimally impact FESS degradation [35]. Given that the lifespan of the FESS at appropriate voltage levels and the maximum operating temperature is typically specified by manufacturers, it is a fair assumption that the FESS will operate under standard operating conditions and endure its projected lifespan in integrated microgrids. Reflecting on the stated aspects, it is reasonable that the FESS degradation cost is excluded from the utilized approach.

Battery lifetime degradation hinges on two primary perspectives. The first one is capacity wear, which pertains to the amount of usable energy. The second is cycling parameters, including the frequency of (dis)charge cycles, cycle life aging, and (dis)charging rates, which indicate inappropriate cycling can lead to battery failure from accelerated degradation [37]. In addition to these two aspects, ambient temperature and the state of charge (SOC) can also adversely affect battery life. The degradation process is accelerated at high temperatures, and extremely high or low SOC levels can severely impair the battery's (dis)charging performance. SOC is described as the remaining energy relative to the total capacity of the BESS in this research. However, temperature controllers are commonly integrated into the BESS in practical applications. Thus, it is presumed that BESS degradation due to ambient temperatures is not considered [38]. For these reasons, the main factors influencing BESS degradation are the depth of discharge (DOD) [39] and cycle life, $N_{CL}(t, \Delta t)$ [40], which is defined as:

$$DOD(t,\Delta t)=\frac{P_{BESS}(t)\Delta t}{C_{BESS}}\times 100\% \quad (5)$$

$$N_{CL}(t,\Delta t)=\alpha_1 DOD(t,\Delta t)^{-\alpha_2}e^{\alpha_3(1-DOD(t,\Delta t))} \quad (6)$$

where $P_{BESS}(t)$ marks the (dis)charging power of BESS at time t, C_{BESS} denotes the BESS capacity, Δt is the time interval for the (dis)charging event, and α_1, α_2 and α_3 are the curve-fitting coefficients of the cycle life-DOD curve. With the obtained DOD and cycle life, the BESS degradation cost can be modeled under two sensible assumptions, the first one is degradation costs for each (dis)charging cycle remain consistent across various levels of SOC, provided the DOD level is unchanged. The second one considers the identical degradation impact on BESS, which treats the degradation cost of charging events as equal to the degradation cost of discharging events, and the BESS degradation cost is [39]:

$$C_{DC}(t,\Delta t)=\frac{K_{BESS}\left|P_{BESS}(t)\right|\Delta t}{2\eta_{BESSCh}N_{CL}(t,\Delta t)C_{BESS}DOD(t,\Delta t)} \quad t\in\{t_{LL},t_{UL}\},\Delta t\in\{\Delta t_{LL},\Delta t_{UL}\} \tag{7}$$

where K_{BESS} stands for the cost of BESS and η_{BESSCh} ($\eta_{BESSDCh}$) is the BESS (dis)charging efficiency; t_{LL} and Δt_{LL} are the current time and time interval in the lower-level control; and t_{UL} and Δt_{UL} are the current time and time interval for the upper-level control.

IV. Utilized Hierarchical Predictive Control Approach

Considering the complementary features of BESS and FESS, this section introduces the hierarchical predictive control approach to enhance the economical and reliable performance of WEVEN with integrated microgrids. The objective of the utilized approach is to optimize the power distribution for integrated microgrids while adhering to operational constraints under RES uncertainties. Specifically, the utilized approach addresses a discrete-time optimization problem within the model predictive control (MPC) framework, where RES uncertainties can be mitigated through the mechanism of utilizing control references from the upper-level control and receiving feedback of state variables from the lower-level control. Control actions for each time interval are determined by solving the objective function specific to each control level, with the decisions of the upper-level control impacting the lower-level control and vice versa.

A. Mathematical Framework for State Dynamics

The state dynamics of the utilized approach must be defined for both the BESS and FESS regarding their (dis)charging power and capacities in both upper and lower control levels. Taking into account the (dis)charging efficiencies, the discrete-time state dynamics equations for the BESS and FESS can be expressed as follows:

$$E_{BESS}(t,\Delta t)=E_{BESS}(t-1)-\frac{P_{BESS}(t)\Delta t}{\eta_{BESSDch}} \quad \text{for } P_{BESS}(t)>0 \tag{8}$$

$$E_{BESS}(t,\Delta t)=E_{BESS}(t-1)-\eta_{BESSCh}P_{BESS}(t)\Delta t \quad \text{for } P_{BESS}(t)<0 \tag{9}$$

$$E_{FESS}(t_{LL},\Delta t_{LL})=E_{FESS}(t_{LL}-1)-\frac{P_{FESS}(t_{LL})\Delta t_{LL}}{\eta_{FESSDCh}} \quad \text{for } P_{FESS}(t_{LL})>0 \tag{10}$$

$$E_{FESS}(t_{LL},\Delta t_{LL})=E_{FESS}(t_{LL}-1)-\eta_{FESSCh}P_{FESS}(t_{LL})\Delta t_{LL} \quad \text{for } P_{FESS}(t_{LL})<0 \tag{11}$$

where $t\in\{t_{LL},t_{UL}\},\Delta t\in\{\Delta t_{LL},\Delta t_{UL}\}$; $E_{BESS}(t,\Delta t)$ and $E_{FESS}(t_{LL},\Delta t_{LL})$ denote the energy status of the BESS and FESS; $P_{FESS}(t_{LL})$ represents the FESS (dis)charging power at time t_{LL}; η_{FESSCh} ($\eta_{FESSDCh}$) is defined as the (dis)charging efficiency of FESS.

B. Control Constraints Formulation

In the utilized approach, power balance constraints must be maintained for both upper and lower control levels:

$$P_{DWCEVs}(t)=P_{Wind}(t)+P_{Solar}(t)+P_{BESS}(t)+P_{FESS}(t_{LL})+P_G(t) \quad t\in\{t_{LL},t_{UL}\} \tag{12}$$

where $P_G(t)$ denotes the power obtained from or sold to the main grid. Plus, the power constraints of the BESS, FESS and main grid are defined as follows:

$$P_{BESS,Min}\le P_{BESS}(t)\le P_{BESS,Max},t\in\{t_{LL},t_{UL}\} \tag{13}$$

$$P_{FESS,Min}(t_{LL})\le P_{FESS}(t_{LL})\le P_{FESS,Max}(t_{LL}) \tag{14}$$

$$P_{G,Min}\le P_G(t)\le P_{G,Max},t\in\{t_{LL},t_{UL}\} \tag{15}$$

where $P_{BESS,Min}$ and $P_{BESS,Max}$ are the BESS lower and upper power limits. $P_{FESS,Min}$ and $P_{FESS,Max}$ are the lower and upper power limits of the FESS. $P_{G,Min}$ and $P_{G,Max}$ are the lower and upper limits for power obtained from or sold to the main grid, while $P_{G,Min}$ can be negative when integrated microgrids are permitted to sell electricity back to the main grid. To avoid over-(dis)charging the BESS and FESS, their SOC limits are:

$$SOC_{BESS,Min}\le\frac{E_{BESS}(t,\Delta t)}{C_{BESS}}\le SOC_{BESS,Max} \tag{16}$$

$$SOC_{FESS,Min}\le\frac{E_{FESS}(t_{LL},\Delta t_{LL})}{C_{FESS}}\le SOC_{FESS,Max} \quad t\in\{t_{LL},t_{UL}\},\Delta t\in\{\Delta t_{LL},\Delta t_{UL}\} \tag{17}$$

where $SOC_{BESS,Min}$ and $SOC_{BESS,Max}$ stand for the minimum and maximum SOC for the BESS. $SOC_{FESS,Max}$ and $SOC_{FESS,Min}$ represent the maximum and minimum SOC for the FESS.

C. Mathematical Framework for Upper-Level Control

Fig. 3 demonstrates the utilized hierarchical predictive control approach, where T_{UL} represents the length of the prediction horizon in the upper-level control. The upper-level control features a nonlinear receding MPC with a time horizon from t_{UL}=1 to t_{UL}=T_{UL}. At present, the optimal scheduling is determined in the upper-level control based on the predicted RES outputs with uncertainties, the charging load of DWC EVs, and time-of-use (TOU) electricity tariffs. The upper-level control actions within Δt_{UL}, namely $P_G(t_{UL})$ and $P_{BESS}(t_{UL})$, are used as reference values to guide control actions in the lower-level control. Using the modeling techniques described in the third section, the objective of the upper-level control is to optimize the decision variables $P_{BESS}(t_{UL})$ and $P_G(t_{UL})$ for simultaneously minimizing the energy cost from the main grid and the BESS degradation cost of integrated microgrids. The energy cost of the WEVEN with integrated microgrids, is defined as $C_G(t_{UL}, \Delta t_{UL})$, which is equivalently the cost of electricity supplied to the WEVEN from the main grid minus the revenues for electricity sold back to the main grid. It is expressed as the summation of these two equations:

$$C_G(t_{UL},\Delta t_{UL})=N_{MG}P_G(t_{UL})\Delta t_{UL}P_{TOU,obtainted} \quad \text{for } P_G(t_{UL})\ge 0 \tag{18}$$

$$C_G(t_{UL},\Delta t_{UL})=N_{MG}P_G(t_{UL})\Delta t_{UL}P_{TOU,sold} \quad \text{for } P_G(t_{UL})<0 \tag{19}$$

where N_{MG} is the number of integrated microgrids in the WEVEN. When $P_G(t_{UL})$ is greater than zero, the integrated microgrid obtains electricity from the main grid, while the microgrid gives electricity back to the main grid when $P_G(t_{UL})$

is below zero. $P_{TOU,obtained}$ and $P_{TOU,sold}$ are the corresponding TOU tariffs for these two situations. By incorporating the energy cost and the BESS degradation cost, $C_{DC}(t_{UL}, \Delta t_{UL})$, into the objective function, the optimization problem in the upper-level control becomes a nonlinear programming problem due to the highly nonlinear nature of the BESS degradation cost. The optimization problem f_{UL} is:

$$f_{UL}: \min \sum_{t_{UL}\in\{1,\ldots,T_{UL}\}} C_{DC}(t_{UL},\Delta t_{UL}) + \sum_{t_{UL}\in\{1,\ldots,T_{UL}\}} C_G(t_{UL},\Delta t_{UL}) \quad (20)$$

under constraints of (7), (8), (9), (12), (13), (15), (16), (18), (19), with variables: $P_{BESS}(t_{UL})$, $P_G(t_{UL})$.

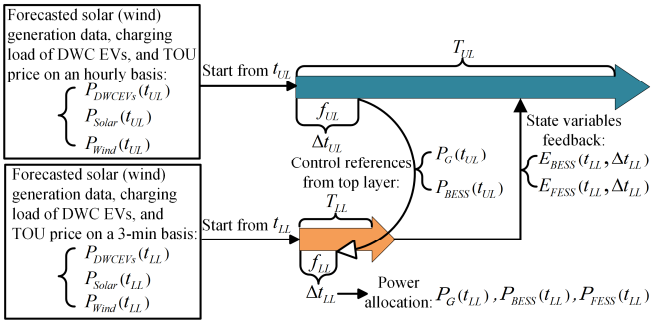

Fig. 3. Structure of utilized hierarchical predictive control approach.

D. Mathematical Framework for Lower-Level Control

For the lower-level control approach, T_{LL} designates the length of the prediction horizon. The lower-level control incorporates a quadratic MPC with the time horizon from t_{LL}=1 to t_{LL}=T_{LL}. The optimization with the FESS implementation in the lower-level control minimizes power fluctuations and further reduces BESS degradation costs within Δt_{LL} of the lower-level control horizon. After each time interval Δt_{UL}, the lower-level control sends the updated state variables $E_{BESS}(t_{LL}, \Delta t_{LL})$ and $E_{FESS}(t_{LL}, \Delta t_{LL})$ back to the upper-level control, and the power dispatch begins for the next time interval Δt_{UL}. One of the objectives of the lower-level control is to control the decision variables $P_{BESS}(t_{LL})$, $P_{FESS}(t_{LL})$ and $P_G(t_{LL})$ to minimize the fluctuations caused by RES uncertainties, thereby ensuring a more reliable operation of the WEVEN integrating microgrids. To achieve this, penalty costs, reflecting deviations from the references set by the upper-level control, are incorporated into the objective function. These penalty terms indicate the discrepancies in power references for the main grid and BESS, caused by RES uncertainties over shorter time intervals. Based on the upper-level control's power references, these penalty costs, $C_{G,PEN}(t_{LL})$ and $C_{BESS,PEN}(t_{LL})$, can be expressed as quadratic functions:

$$C_{G,PEN}(t_{LL}) = (P_G(t_{LL}) - P_G(t_{UL}))^2 \quad (21)$$

$$C_{BESS,PEN}(t_{LL}) = (P_{BESS}(t_{LL}) - P_{BESS}(t_{UL}))^2 \quad (22)$$

The BESS degradation cost, $C_{DC}(t_{LL}, \Delta t_{LL})$, should also be integrated into the lower-level control objective to promote more economical operations of the WEVEN with integrated microgrids. The optimization problem, f_{LL}, in the lower-level control, can be expressed as a quadratic programming problem:

$$f_{LL}: \min \sum_{t_{LL}\in\{1,\ldots,T_{LL}\}} (C_{G,PEN}(t_{LL}) + C_{BESS,PEN}(t_{LL})) + \sum_{t_{LL}\in\{1,\ldots,T_{LL}\}} C_{DC}(t_{LL},\Delta t_{LL}) \quad (23)$$

under constraints of (7), (8)-(17), (21), (22), with variables: $P_{BESS}(t_{LL})$, $P_{FESS}(t_{LL})$, $P_G(t_{LL})$.

V. Performance Studies

A. Simulation Settings

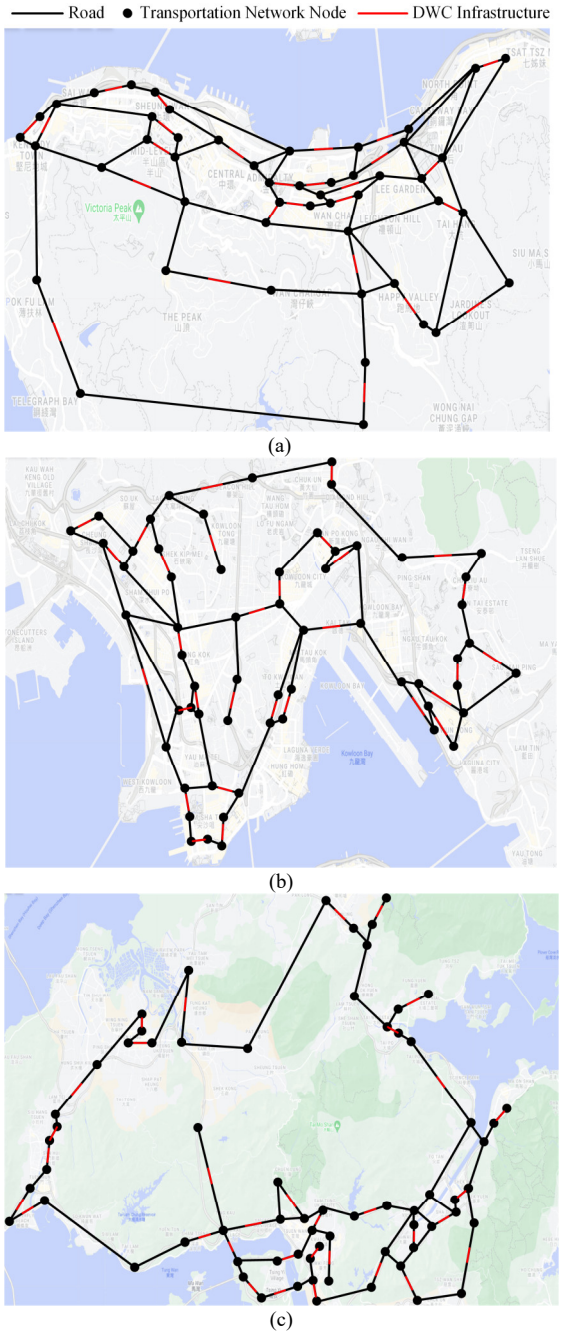

Fig. 4. WEVEN with link-based transportation network model across Hong Kong's three sub-territories: (a) Hong Kong Island. (b) Kowloon. and (c) New Territories.

This section showcases the utilized hierarchical predictive control approach under various RES FEs. Its performance is evaluated against benchmark control strategies in the current research from three perspectives: the energy cost, BESS degradation cost, and EENS of the WEVEN with integrated

microgrids. The utilized approach is executed in MATLAB, with the optimizations at both the upper and lower control levels solved using the IPOPT (Interior Point Optimizer) solver. The simulation is performed over a 24-hour scheduling horizon, and the parameters used are detailed in Table I, where the time intervals and prediction horizon are set to 1 hour and 24 hours for the upper-level control, and 3 minutes and 1 hour for the lower-level control. The RES FEs are modeled with 10% to 25% discrete Gaussian distributed random variables [32] [33]. For TOU tariffs, it is 0.753 $/kWh during peak hours (hours 9-21) and 0.676 $/kWh during off-peak hours (hours 22-8) [41]. When integrated microgrids return energy to the main grid, the selling electricity tariff is set as 90% of regular TOU tariffs.

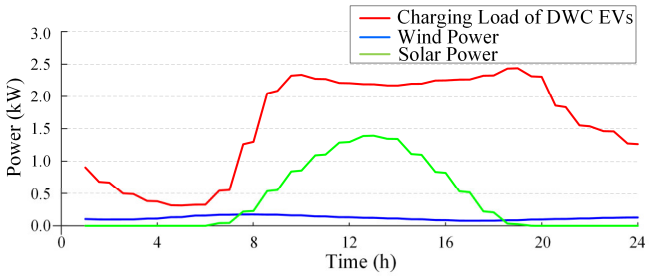

Fig. 5. Seasonal DWC EVs' charging load, exact solar and wind power for integrated microgrid in WEVEN of 24 hours, Spring as an example.

In the WEVEN of interest, each DWC infrastructure is integrated with a microgrid equipped with RES and HESS. The parameters of the DWC infrastructure are presented in Table II. The length of DWC lanes within the DWC infrastructure is set as 100 m, and the maximum DWC power is 20 kW [42]. The WEVEN is spread across Hong Kong's three sub-territories: Hong Kong Island (HK), Kowloon (KL), and New Territories (NT) based on the link-based transportation network model as shown in Fig. 4 according to traffic counting core stations' locations [43]. The total number of DWC infrastructures (WEVEN-integrated microgrids) in the WEVEN is consistent with the number of core traffic-counting stations presented in the Hong Kong government's annual traffic census, which is 117 [43]. The average vehicle speed within each sub-territory is also shown to calculate the charging load of DWC EVs.

TABLE I
SIMULATION PARAMETERS

Parameters	T_{UL} hr	Δt_{UL} hr	T_{LL} min	Δt_{LL} min	FEs %	$P_{TOU,\,obtained}$ $/kWh
Values	24	1	60	3	10-25	0.753 0.676

TABLE II
PARAMETERS OF DWC INFRASTRUCTURES

Parameters	L km	P_{DWC} kW	V(HK) km/h	V(KL) km/h	V(NT) km/h	N_{MG} No.
Values	0.1	20	23.5	22.9	39.8	117

To accurately model the charging load of DWC EVs in the DWC infrastructure of the WEVEN, the seasonal factor k is adopted to reflect the traffic pattern's seasonal variations, and the hourly total number of DWC EVs traversing on DWC lanes is calculated average using the link-based transportation network model and time-dependent link-loading transportation flow model [24] following core traffic counting stations' traffic volume data [43]. Likewise, α_{EV} is set to 9% according to the Hong Kong Environmental Protection Department, and α_{DWCEV} is set at 15% [44]. The seasonal charging load of DWC EVs for the integrated microgrid in 24 hours using Spring as an example, can be seen in Fig. 5. The parameters for HESS are presented in Table III and Table IV, where the BESS's power limit is 5 kW with a capacity of 10 kWh. To address the BESS degradation cost for promoting the economical operation of the WEVEN with integrated microgrids, the BESS is protected from over-(dis) charging by setting its SOC limit from 20% to 80%. The cost of the BESS is 180 $/kWh with the (dis)charging efficiency being 95%, and 3142, 1.6 and 0.000087 are used as cycle life-DOD curve fitting coefficients [40]. The upper power limit and capacity for FESS are 15 kW and 5 kWh, with a (dis)charging efficiency of 85% [35]. To balance the instant power mismatch and alleviate the (dis)charging stress on the BESS, upper (lower) limits of FESS SOC are 0% and 100%.

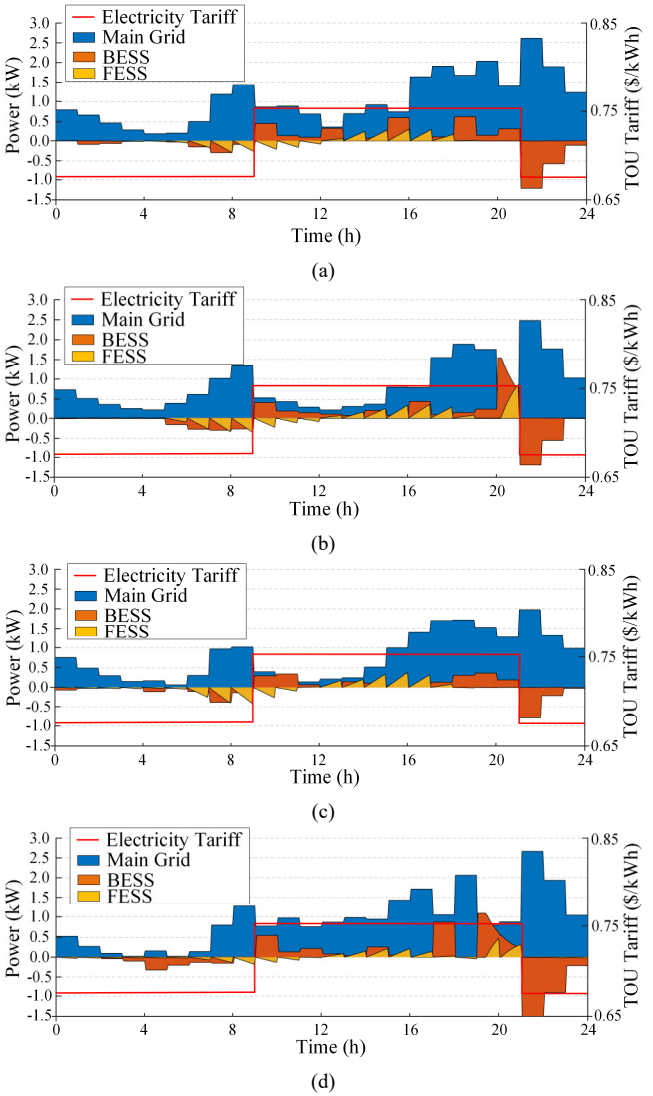

Fig. 6. Seasonal daily optimal power dispatches of integrated microgrid by utilizing hierarchical predictive control approach. (a) Spring. (b) Summer. (c) Autumn. (d) Winter.

To emulate RES outputs in the integrated microgrid, the

seasonal hourly wind speed and total all-sky surface photosynthetically active radiation are obtained through the NASA world geocoding service database, with the location selected as Hong Kong. The installed capacity of photovoltaic systems for the integrated microgrid is 2.5 kW, with an efficiency of 95% [28]. The wind turbine rotor diameter in the integrated microgrid is set to 2m, where the density of air and coefficient of performance are set as 1.225 kg/m^3 and 0.593. The exact seasonal solar and wind power generation of the integrated microgrid for 24 hours using Spring as an example, is also detailed in Fig. 5.

TABLE III
PARAMETERS OF HESS IN WEVEN-INTEGRATED MICROGRIDS

Parameters	$P_{BESS/FESS}$ kW	$C_{BESS/FESS}$ kWh	$K_{BESS/FESS}$ \$/kWh	α_1	α_2	α_3
BESS	5	10	180	3142	1.6	0.000087
FESS	15	5	N.A.	N.A.	N.A.	N.A.

TABLE IV
SOC AND EFFICIENCY OF HESS IN WEVEN-INTEGRATED MICROGRIDS

Parameters	$\eta_{BESSCh/FESSCh}$ %	$\eta_{BESSDCh/FESSDCh}$ %	SOC_{Min} %	SOC_{Max} %
BESS	95	95	20	80
FESS	85	85	0	100

B. Optimal Power Dispatch of Utilized Approach

Fig. 6 illustrates the seasonal daily optimal power dispatches for the integrated microgrid according to TOU tariffs determined by the utilized hierarchical predictive control approach. As anticipated, the BESS operation is primarily regulated by TOU tariffs in the upper-level control, with the BESS discharging during peak times and charging during off-peak times. Fig. 6 also shows that the lower-level control addresses hourly fluctuations of RES, stabilizing the power variations of the BESS and the main grid within small ranges, which promotes the system's reliability. Meanwhile, the FESS is frequently (dis)charged at high rates to smooth out uncertainties of RES outputs and DWC EVs' charging load.

C. Benchmark Comparison and Case Evaluations

1) Benchmark Configurations: Besides the collaborative predictive control approach [14], the optimal control method employing non-dominated sorting genetic algorithms (NSGA) is also common and effective in dealing with the strategic scheduling of electric vehicle-based microgrids [23]. Thus, both approaches serve as comparative benchmarks to assess the advantages and performance of the utilized hierarchical predictive control approach for the WEVEN with integrated microgrids. For comparative benchmarks, the entire HESS operates only at one single control level. To be more specific, the collaborative predictive control benchmark shares the same structure and parameters with the upper-level control of the utilized hierarchical predictive control approach, which are listed in Table I. For both the collaborative predictive control and optimal control with NSGA benchmarks, they share the same configurations regarding the DWC infrastructures and HESS with the utilized hierarchical predictive control approach, as shown in Table II, III, and IV. For the optimal control with NSGA benchmark, its specific parameters are shown in Table V. The comparative cases are examined under the utilized and benchmark control approaches regarding three aspects: energy cost, BESS degradation cost, and EENS of the WEVEN with integrated microgrids.

2) Power Comparison Studies: Since the direct results from the above-stated utilized approach and comparative benchmark approaches are powers from the main grid, BESS, and FESS. Also, the subsequent energy costs, BESS degradation costs, and EENS are calculated from these power levels. Thus, detailed power comparison studies are conducted here. However, only the power comparison results for spring with RES FEs of 0%, 15%, and 25%, are shown in Fig. 7 due to the page limit.

TABLE V
KEY PARAMETERS OF BENCHMARK: OPTIMAL CONTROL WITH NSGA

Variable	**Value**
Population size	200
Crossover probability	0.9
Mutation probability	0.1
Maximum number of generations	1000
Mutation strength	0.05

From these power comparison plots, the first column is the power comparison from the main grid under different FEs, it can be observed that the power curves from the collaborative predictive control and optimal control benchmark are more fluctuated than the power curves from the utilized method, they even have some spikes at specific time spots, thus leading to higher energy costs and less reliability compared with the utilized approach. The subplots in the second column are the comparison of BESS power under various FEs. From these subplots, it is noticeable that the power curves from the utilized method are more alleviated than the power curves from the two comparative control benchmarks, thus contributing to the more optimized BESS degradation costs. As for the third column, these are the comparison results of the power level from FESS. It is evident that the power curves from the utilized approach have more frequent and larger magnitude charging/discharging than the power curves of the collaborative predictive control benchmark. This indicates the utilized method utilizes FESS more often than the comparative control benchmarks to compensate for the power imbalance, thus further promoting economical and reliable operations. Also, power comparisons from spring with 10% and 20% FEs, and all the other seasons with varied FE levels, show similar trends to the spring results. Thus, from this power comparative study, the utilized method maintains superior cost performance and reliability regardless of RES FEs, further validating its effectiveness.

3) Energy Cost: The seasonal energy cost of the WEVEN with integrated microgrids for 24 hours, defined by the summation of (18) and (19), is compared using benchmark and utilized control approaches under various RES FEs. The comparison results are shown in Fig. 8, where it can be observed that the seasonal daily energy cost varies with seasons since the optimal power dispatch within integrated microgrids changes due to different seasonal charging loads of DWC EVs and RES outputs. As the figures depict, all the seasonal daily energy costs from the utilized approach are lower than those for comparative benchmark control strategies

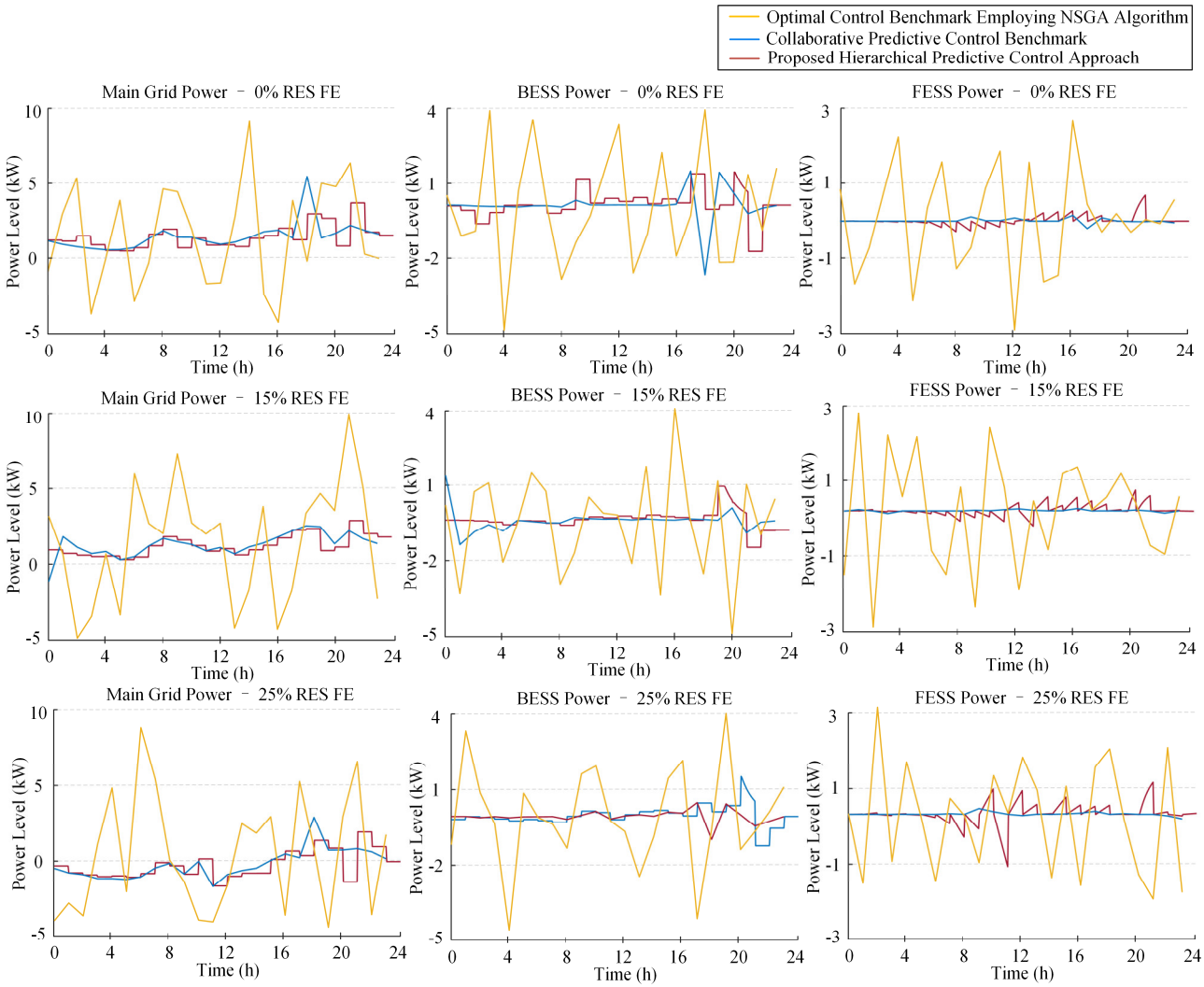

Fig. 7. Power comparisons from main grid, BESS, FESS for Spring under various RES FEs.

with varied RES FEs. The seasonal daily energy cost difference ranges from 12$ to 1302$, averaging 419$. By employing the longer time frame in the upper-level control of the utilized approach, the seasonal daily energy cost for the WEVEN with integrated microgrids is reduced compared with the benchmark control strategies, thus contributing to the more economical operation of the WEVEN with integrated microgrids in the presence of RES uncertainties.

4) BESS Degradation Cost: Under different RES FEs, the seasonal BESS degradation cost for WEVEN with integrated microgrids, as outlined in (7), is compared over 24 hours using both the utilized and benchmark control strategies, as illustrated in Fig. 9.

Due to the varying seasonal RES outputs and charging loads of DWC EVs, the seasonal daily BESS degradation cost also alters with the seasons, as the optimal power distribution of integrated microgrids shifts. As shown in the figures, with different FEs of RES, the seasonal daily BESS degradation costs using the benchmark collaborative predictive control strategy and the optimal control benchmark are significantly higher than those observed with the utilized approach, with differences falling between 9$ and 1.47$ and the average of 6.19$. This is achieved by utilizing both the longer and shorter time frames in the upper and lower control levels of the utilized approach, which further contributes to the more economical operation of the WEVEN with integrated microgrids, even with the disturbance of RES uncertainties.

5) EENS: Expected energy not served is a typical reliability assessment parameter to assess the amount of unmet load demand of an energy system [13], which can be calculated for the WEVEN with integrated microgrids as follows:

$$EENS = N_{season} N_{MG} \sum_{t_{UL}=1}^{t_{UL}=T_{UL}} \max(0,(P_{Wind}(t_{UL}) + P_{Solar}(t_{UL}) + P_G(t_{UL}) + \max(0,P_{BESS}(t_{UL})) + \max(0,P_{FESS}(t_{UL})) - P_{DWCEVs}(t_{UL}) - \max(0,-P_{BESS}(t_{UL})) - \max(0,-P_{FESS}(t_{UL})))\Delta t_{UL} \quad (24)$$

From (24), EENS can be calculated for the comparative benchmark control strategies. The same equation is used to calculate EENS for the utilized approach but with the time horizon and time interval of the lower-level control. The minus sign indicates that the BESS or FESS is charging and should be treated as a load. Conversely, the positive sign

means they discharge and act as generation units. N_{season} represents the number of days in each season.

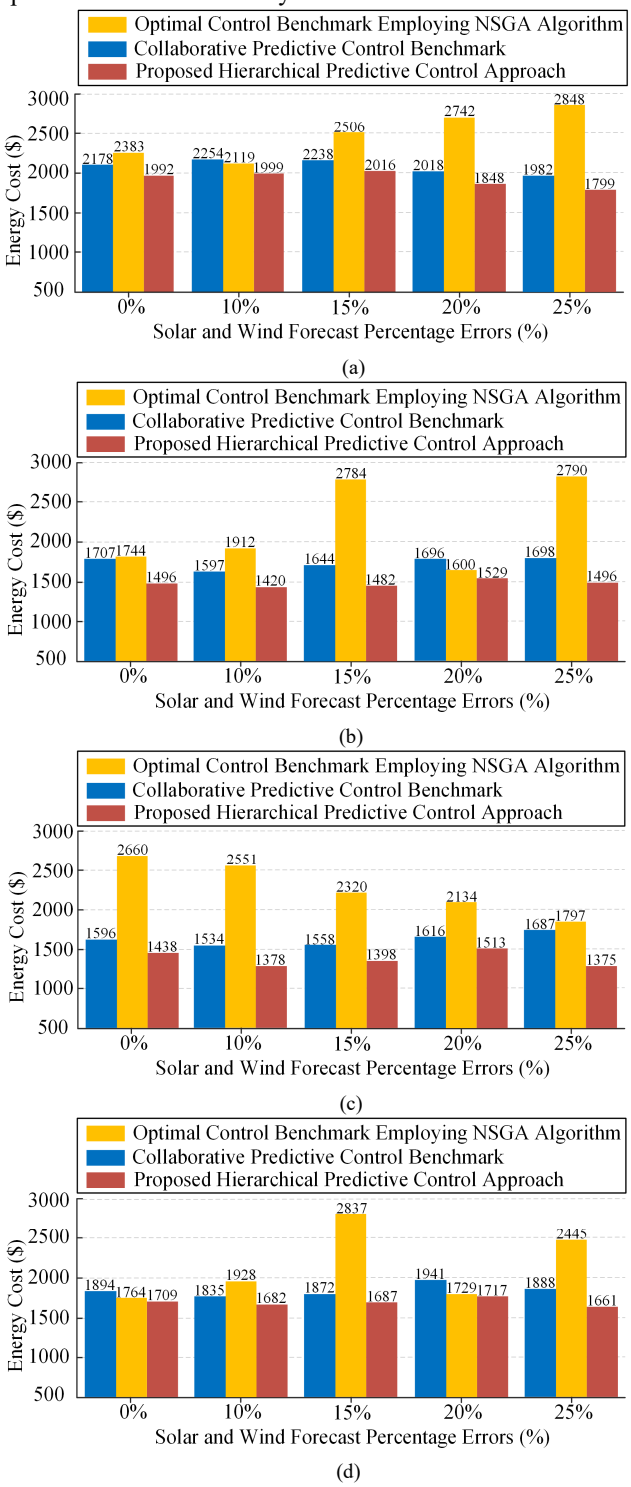

Fig. 8. Seasonal energy cost of WEVEN with integrated microgrids for 24 hours under various RES FEs. (a) Spring. (b) Summer. (c) Autumn. (d) Winter.

The EENS comparative results are depicted in Fig. 10, where seasonal EENS from the utilized approach and the optimal control benchmark are zero, indicating that all the load demand of the WEVEN with integrated microgrids is satisfied. Nonetheless, seasonal EENS from the collaborative predictive control benchmark is not zero and increases with the growing RES FEs due to higher inaccuracies in renewable energy prediction, increased volatility in RES outputs, and potential insufficient reserve capacity to handle unexpected power imbalances. Hence, the utilized hierarchical predictive control approach can indeed offer better reliability to the WEVEN with integrated microgrids.

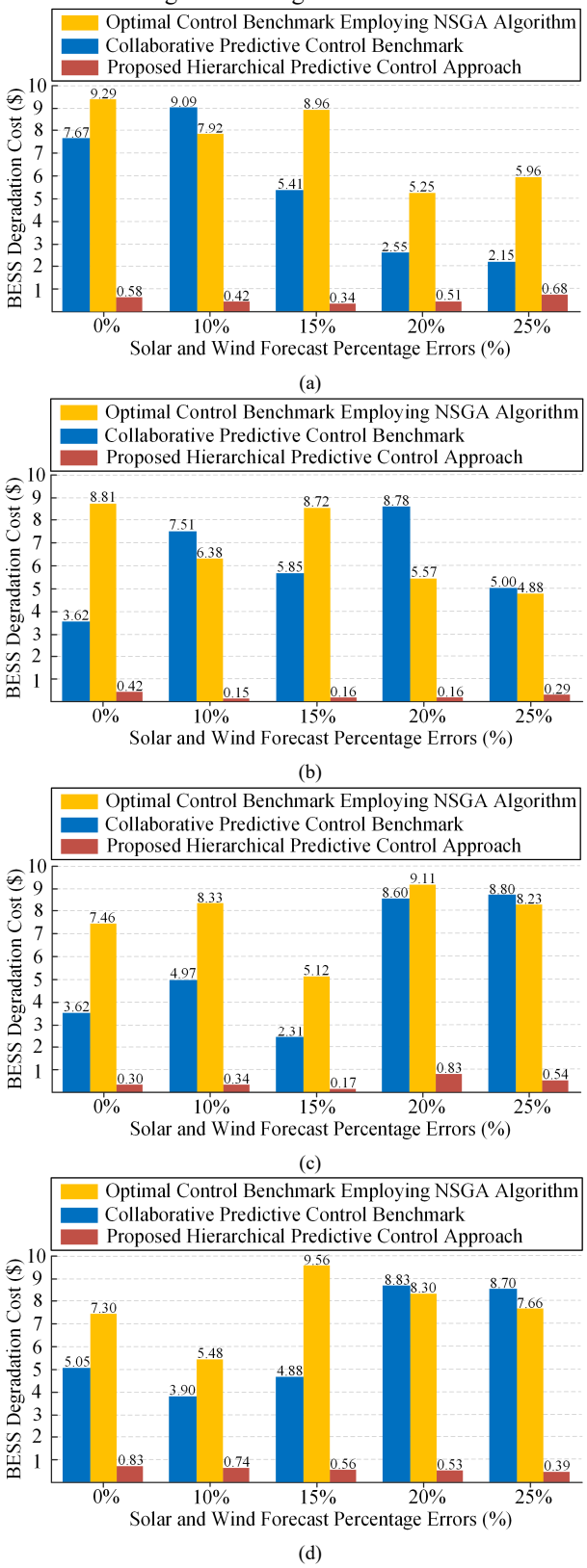

Fig. 9. Seasonal BESS degradation cost for WEVEN with integrated microgrids over 24 hours under differed FEs of RES. (a) Spring. (b) Summer. (c) Autumn. (d) Winter.

Based on the above comparisons from three facets, it is evident that single-level comparative control benchmarks might not adequately achieve optimal power dispatch for HESS with distinctive features in WEVEN with integrated microgrids, particularly for BESS and FESS in this study. Thus, single-level comparative control benchmarks might not effectively handle HESS functionalities. Instead, the hierarchical predictive control approach is deliberately designed to separate operation modes across various time frames in different control levels, addressing diverse characteristics of ESS with better performance.

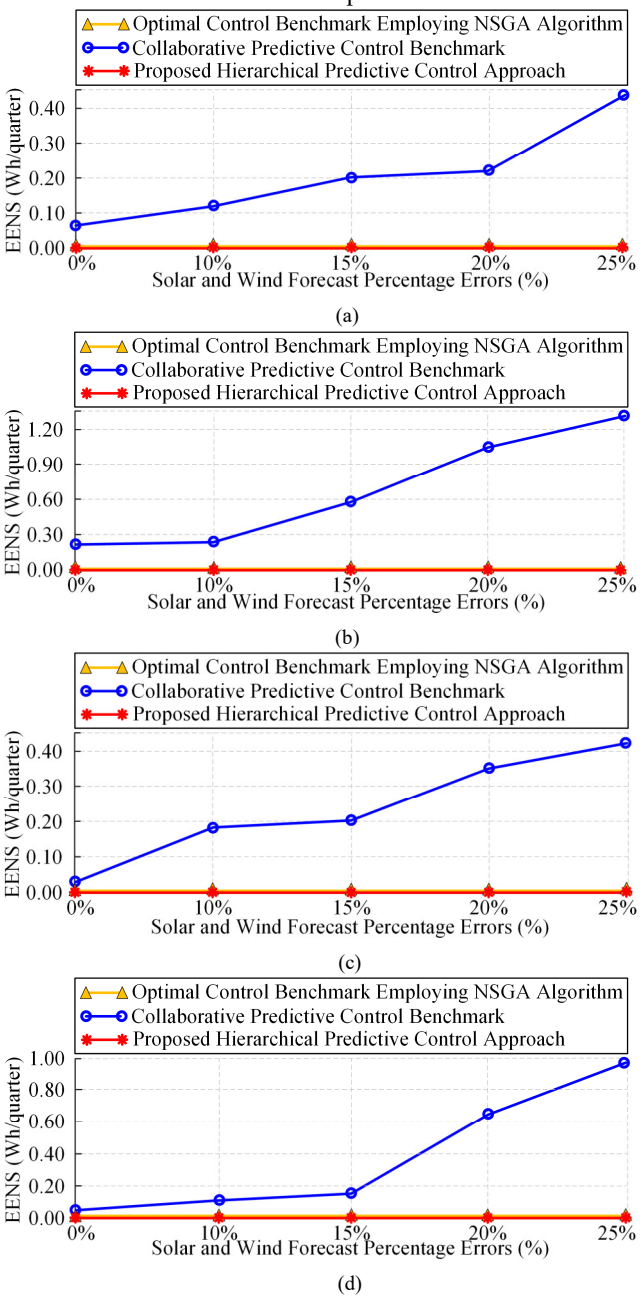

Fig. 10. Seasonal EENS for the WEVEN with integrated microgrids under different RES FEs. (a) Spring. (b) Summer. (c) Autumn. (d) Winter.

As stated earlier, the linkage between WEVEN and microgrids remains unaddressed in [14]–[22]. Also, critical limitations further include: BESS degradation costs are unaccounted for in [14]–[18], [20]–[22], RES forecasting uncertainties are unmodeled in [16], [19], [21], and [21] [22] omits reliability. From the above detailed analysis of research results in this section, these empirical results substantiate that the utilized method not only considers things that are neglected in the literature review, but also shows its effectiveness in these neglected aspects in terms of more economical and reliable operations for the given system of interest.

D.Statistical Analysis of Research Results

In order to demonstrate the significance of the research results, the statistical analysis approach named null hypothesis significance testing should be used [45]. Among various null hypothesis significance testing methods, the two-way Analysis of Variance (ANOVA) is suitable for this research, since the research data is with structured factorial design with two independent factors (RES FE levels and control approaches), each measured at multiple levels, enables the two-way ANOVA to statistically quantify their individual effects on energy costs, degradation costs, and EENS, thus showing the statistical siginificance of research results [46]. The two-way ANOVA is performed for each season with respect to energy costs, BESS degradation costs, and EENS. For all the two-way ANOVA analyses, 0.05 is used as the significance level reference.

1) Energy Cost:

TABLE VI
P-VALUES OF ENERGY COST

P-values	RES FEs	Control Approaches
Spring	0.9679	0.0100
Summer	0.4724	0.0317
Autumn	0.6296	0.0005
Winter	0.5316	0.1022

Taking spring as an example, the null hypothesis H_0 for the first factor (RES FE levels), is that all mean spring energy costs are equal across RES FE levels. Because the p-value is 0.9679 for the first factor, which far exceeds the significance level of 0.05, this indicates it fails to reject H_0, which means RES FEs do not significantly affect spring energy costs. Even large errors (e.g., 25%) don't systematically increase/decrease spring energy costs. For the second factor (control approaches), the null hypothesis H_0: all mean spring energy costs are equal for the three control approaches. Since the p-value is 0.0100 for the second factor, which is less than the significance level of 0.05, this indicates it rejects H_0, which means the utilized approach consistently has the lowest energy costs across all RES FE levels. These statistical analysis results also show that the control approach choice impacts spring energy costs more than RES FEs.

According to the p-values for all four seasons, all the p-values from the factor of RES FEs far exceed the significance level reference, and the p-values for spring, summer, and autumn from the factor of control approaches are less than the significance level reference, indicating RES FEs do not significantly affect energy costs, but method choice does, with

the utilized method consistently achieves the lowest energy costs across all FE levels. Although the p-value for winter from the second factor is slightly greater than the significance level reference, the absence of significant interaction confirms that this superiority pattern still holds regardless of RES FEs. This statistical evidence collectively demonstrates the effectiveness of the utilized approach, which also indicates its statistically robust performance on economical operations.

2) BESS Degradation Cost:

TABLE VII
P-VALUES OF BESS DEGRADATION COST

P-values	RES FEs	Control Approaches
Spring	0.1381	0.0006
Summer	0.8210	0.0006
Autumn	0.0770	0.0001
Winter	0.3447	0.0002

Also using spring as an illustrative case, the null hypothesis H_0 for RES FEs asserts that mean BESS degradation costs for spring remain consistent across all FE levels. With a p-value of 0.1381—well above the 0.05 significance threshold—this hypothesis cannot be rejected, indicating that RES FEs do not meaningfully impact degradation costs in spring, even at extreme levels like 25%. Conversely, for control methods, the null hypothesis of equal degradation costs across different control methods is strongly rejected ($p = 0.0006$), demonstrating that method selection critically influences outcomes, with the utilized strategy consistently yielding the lowest BESS degradation costs.

This pattern persists universally: RES FEs show no significant effect in any season, while control methods drive highly significant differences in BESS degradation costs across various seasons, which confirms the utilized method's consistent superiority in minimizing BESS degradation costs—irrespective of RES FEs or seasonal variations—solidifying its robust operational advantage with statistical significance.

3) EENS:

TABLE VIII
P-VALUES OF EENS

P-values	RES FEs	Control Approaches
Spring	0.4609	0.0064
Summer	0.4607	0.0088
Autumn	0.4600	0.0034
Winter	0.4605	0.0591

Examining spring as a representative case, the null hypothesis H_0 for RES FEs claims no difference in mean EENS across FE levels. The high p-value (0.4609)—well beyond the 0.05 significance cutoff—fails to reject this hypothesis. This confirms that RES FEs (even at 25%) do not meaningfully alter EENS outcomes. In contrast, control methods show starkly different results: the hypothesis of equal EENS across various approaches is firmly rejected ($p = 0.0064$), proving control methods directly impact EENS, with the utilized strategy consistently achieving superior reliability.

This trend holds universally: RES FEs exhibit no seasonal influence, while control methods drive significant EENS distinctions in all seasons except winter, where results show marginal significance ($p=0.0591$). Critically, the utilized method maintains its robust performance advantage in minimizing EENS regardless of FEs or seasonal shifts, showing its statistically significant operational robustness in energy reliability management.

E. Control Robustness

The analysis in Section V-D confirms the utilized approach's control robustness, as demonstrated by achieving the lowest energy costs, minimal BESS degradation costs, and highest reliability irrespective of different RES FE levels or seasonal variations. Such robustness is collaboratively achieved through different designed mechanisms within the approach, the time-scale separation and the feedback correction. For the first mechanism, the slower time scale in the upper-level control proactively absorbs slow-varying disturbances (e.g., RES generation drift, EV wireless charging demand trends) through re-optimization every hour, and the faster time scale in the lower-level control compensates for transients (e.g., sudden cloud cover) every 3 minutes. This prevents disturbance/error propagation and supports control robustness. For the second mechanism, at each MPC control level, the actual system states are measured, then deviations from predictions are fed back to re-solve optimization problems, correcting trajectories before disturbances/errors accumulate, thus further limiting disturbance/error propagations and contributing to the robustness performance.

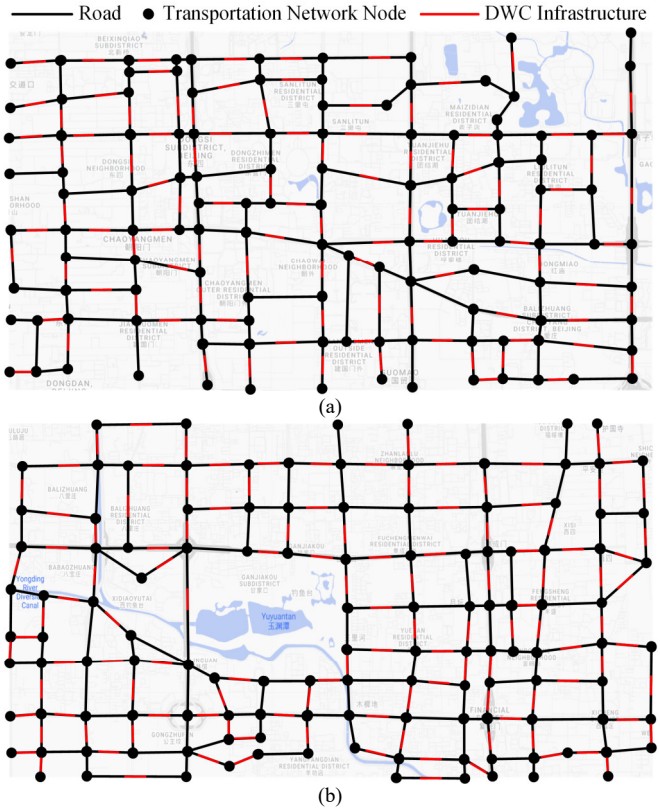

Fig. 11. WEVEN with link-based transportation network model across part of Beijing's four districts: (a) Dongcheng and Chaoyang. (b) Xicheng and Haidian.

F. Scalability

In order to demonstrate the scalability of the utilized approach, it is applied to a larger urban network of Beijing's

actual road network structures and traffic data [47]. To be more specific, 249 DWC infrastructures with associated microgrids are utilized as shown in Fig. 11. Renewable power generation calculations use meteorological data, such as total all-sky surface photosynthetically active radiation and wind speed, obtained from NASA's World Geocoding Service database with location set as Beijing. The TOU electricity tariffs are also set using Beijing's EV electricity prices [48].

The energy cost, degradation cost, and EENS for the larger network in Beijing of spring with varied RES FEs are shown in Fig. 12. The results for other seasons with different RES FEs are not listed here due to page limit. As can be observed, the energy cost of the larger network examined in Beijing is lower than the energy cost of the smaller network examined in Hong Kong, since the TOU tariffs in Hong Kong are much higher than the TOU tariffs of Beijing.

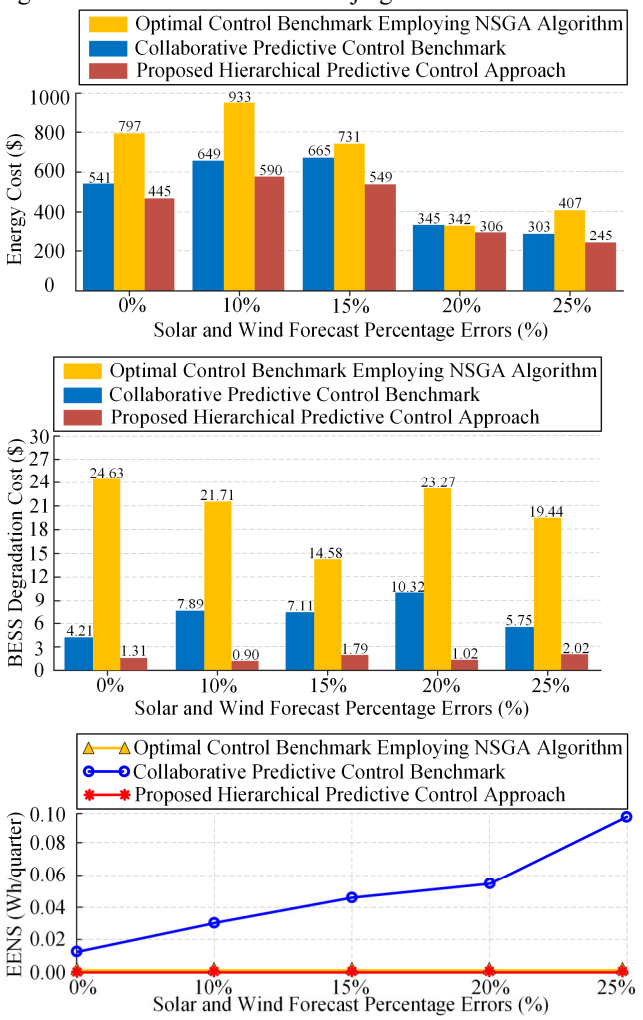

Fig. 12. Energy cost, degradation cost, EENS for larger network of Beijing in Spring with different RES FEs.

For the research results from different seasons with various FEs, the utilized approach yields consistently lower seasonal daily energy costs than all benchmark control strategies. The daily energy cost difference between seasons spans from 36$ to 862$, with an average of 276$. Both the benchmark collaborative predictive control strategy and the optimal control benchmark exhibit markedly higher seasonal daily BESS degradation costs than the utilized approach, with the difference ranging from 0.55$ to 27.63$ and averaging 13.86$. While both the utilized approach and optimal control benchmark achieve zero seasonal EENS, confirming full load satisfaction for the WEVEN with integrated microgrids, the collaborative predictive control benchmark exhibits non-zero EENS, revealing unmet system demand.

To summarize, the utilized approach indeed provides better economic and reliable performance to the WEVEN with integrated microgrids than the benchmark control strategies even for the larger urban network, and this also demonstrates the superior scalability of the research.

G. Hardware-in-the-loop Simulations

To prove the real-world applicability and superiority of the utilized approach, downscale hardware-in-the-loop (HIL) simulations are conducted to emulate the EV wireless charging power from the main grid on the lab scale. In this HIL simulation setup, a WPT system based on the advanced three-level full-bridge inverters is constructed. The key parameters associated with this WPT system are shown in Table IX. The full HIL setup, as depicted in Fig. 13, integrates several key components: an OPAL-RT OP1420 PHIL (Power-Hardware-in-the-loop) microgrid test bench, a WPT charging system, and an electronic load. For the WPT charging system, it consists of a rectifier, a three-level full-bridge inverter, a transmitter coil, and a receiver coil. For hardware design and safety reasons, a maximum power of 0.6kW is implemented for the HIL experiments in the lab environment.

TABLE IX
PARAMETERS OF WPT SYSTEM WITH THREE-LEVEL INVERTER

Items	Value
Resonant frequency	100 kHz
Mutual inductance	25.50 μH
DC bus voltage	150 V
Distance between coils	8 cm
Primary coil inductance	85.38 μH
Secondary coil inductance	84.93 μH
Primary compensated capacitance	30.07 nF
Secondary compensated capacitance	30.58 nF
Digital signal processor	TMS320F28377
SiC MOSFET	SCT3080
Diode	STPSC40G12WL

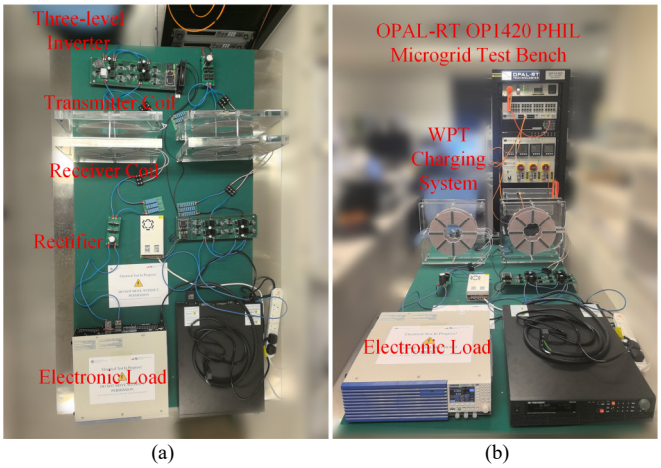

(a) (b)

Fig. 13. System configuration of HIL simulation. (a) Top view. (b) Front view.

The power-level oscillograms of the EV wireless charging power from the main grid are formulated and analyzed with

different RES FEs in all four seasons, under the utilized approach and comparative control benchmarks, from 9:00 AM to 9:03 AM during the morning peak hours in Hong Kong. Due to the page limit, only the power-level oscillogram under the 0% RES FEs in spring is illustrated here in Fig. 14. As it can be observed, the power level from the utilized hierarchical predictive control approach is significantly lower than the power levels from the optimal control and collaborative predictive control benchmarks during the sampled peak load intervals, which demonstrates the effectiveness of the utilized approach in achieving more economical and reliable operations for the given system of interest. Power-level oscillogram comparative studies from all other seasons at different RES FE levels exhibit trends analogous to the spring 0% RES FE result, further underscoring the superiority of the utilized approach.

H. Limitations and Potential Future Works

There are several limitations associated with this research, firstly, the degradation cost function accounts for cycling aging but omits calendar aging, risking underestimation of long-term BESS replacement costs. Also, for the wireless charging, the loss from the misalignment during charging is a practical issue, and it has remained unexamined in the current study. Besides, the continuum modeling of EVs' arrivals and departures may not capture energy demand variability in low traffic density settings, which is common in real life in small cities. Future works may incorporate hybrid modeling techniques, where continuum flows are combined with Poisson-process-based discrete events for low traffic density scenarios. Moreover, exploring effective control and optimization approaches for energy trading inside the WEVEN through DWC-enabled EVs traveling between different DWC infrastructures can serve as interesting and promising future research topics.

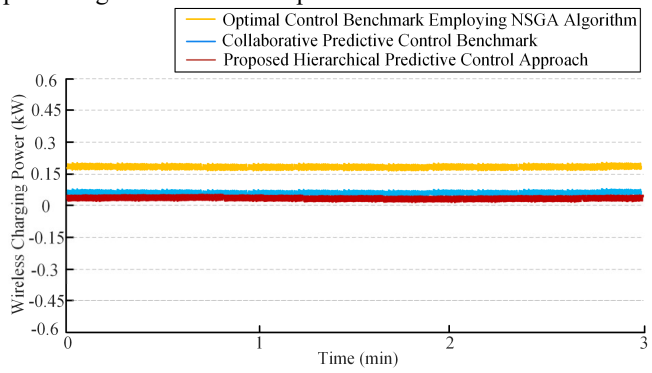

Fig. 14. Power-level oscillograms for WCEVs under different methods in sampled peak load time intervals from downscale HIL experiments (Spring, 0% RES FEs).

VI. Conclusion

This research utilized a hierarchical predictive control approach for the wireless electric vehicle energy network with integrated microgrids considering battery energy storage systems' degradation costs. The wireless electric vehicle energy network includes dynamic wireless charging infrastructures and integrated microgrids that embrace renewable energy sources, hybrid energy storage systems, the charging load of dynamic wireless charging electric vehicles and the point of common coupling connected to the main grid. The utilized approach is designed to ensure economical and reliable operations while accounting for renewable energy sources' uncertainties, including forecast errors, intermittency and power fluctuations. The power dispatch is planned in the upper-level control to address economical operations by reducing the energy and degradation costs. Concurrently, in the lower-level control, the degradation cost is further decreased. System reliability related to renewable energy sources' uncertainties is also improved by minimizing power fluctuations using control references from the upper-level control and state variables feedback from the lower-level control. The degradation cost is modeled and integrated into the utilized approach to transform costs coupled with longer time frames into power dispatch optimizations in shorter time frames, which is required by the inherent distinctive natures of hybrid energy storage systems. Comparative simulations efficiently show that energy storage systems with different features, such as battery energy storage systems and flywheel energy storage systems, can be applied at different control levels to achieve optimal power dispatches of distinct objectives. The method's distinctive novelty lies in synthesizing understudied factors in the current literature, while ensuring better economical and reliable operations for the given system of interest across renewable energy sources' volatility regimes. The feasibility of the utilized approach has been verified, as demonstrated by its superior performance compared with the collaborative predictive control and optimal control benchmarks from multiple perspectives, featuring the reduction of energy costs, degradation costs and expected energy not served, by up to 1302$, 27.63$, and 1.3Wh/quarter respectively. Moreover, an average reduction of energy costs by 348$, degradation costs by 10.03$, and expected energy not served down to 0 Wh/quarter is also achieved through this method.

VII. References

[1] A. Y. S. Lam, K. C. Leung, and V. O. K. Li, "Vehicular energy network," *IEEE Trans. Transp. Electrif.*, vol. 3, no. 2, pp. 392-404, Jun. 2017.

[2] H. Feng, R. Tavakoli, O. C. Onar and Z. Pantic, "Advances in high-power wireless charging systems: Overview and design considerations," *IEEE Trans. Transp. Electrif.*, vol. 3, no. 3, pp. 886-919, Sept. 2020.

[3] Z. Zhou, Z. Liu, H. Su and L. Zhang, "Optimal operation for cross-period scheduling of electric vehicles in traffic-power systems," *IEEE Trans. Transp. Electrif.*, vol. 10, no. 3, pp. 6676-6689, Sept. 2024.

[4] W. Liu, X. Wang, and Y. Xu, "Bilevel planning of wireless charging lanes in coupled transportation and power distribution networks," *IEEE Trans. Transp. Electrif.*, vol. 10, no. 2, pp. 2499-2510, Jun. 2024.

[5] Y. Liu, Y. Xue, Z. Zhou, X. Han, X. Chang, and J. Su, "Coordinated dispatch of power and transportation systems considering hydrogen storage based on heterogeneous decomposition," *IEEE Trans. Transp. Electrif.*, vol. 10, no. 3, pp. 7526-7539, Sept. 2024.

[6] S. Lv, Z. Wei, G. Sun, S. Chen and H. Zang, "Power and traffic nexus: from perspective of power transmission network and electrified highway network," *IEEE Trans. Transp. Electrif.*, vol. 7, no. 2, pp. 566-577, Jun. 2021.

[7] C. C. T. Chow, A. Y. S. Lam, W. Liu, and K. T. Chau, "Multisource–multidestination optimal energy routing in static and time-varying vehicular energy network," *IEEE Internet Things J.*, vol. 9, no. 24, pp. 25487-25505, Dec. 2022.

[8] W. Liu, K. T. Chau, C. C. T. Chow, and C. H. T. Lee, "Wireless energy trading in traffic internet," *IEEE Trans. Power Electron.*, vol. 37, no. 4, pp. 4831-4841, Apr. 2022.

[9] W. Su, J. Wang, and J. Roh, "Stochastic energy scheduling in microgrids with intermittent renewable energy resources," *IEEE Trans. Smart Grid*, vol. 5, no. 4, pp. 1876-1883, Jul. 2014.

[10] T. Wu, Q. Yang, Z. Bao, and W. Yan, "Coordinated energy dispatching in microgrid with wind power generation and plug-in electric vehicles," *IEEE Trans. Smart Grid*, vol. 4, no. 3, pp. 1453-1463, Sept. 2013.

[11] K. B. Kwon, and H. Zhu, "Reinforcement learning-based optimal battery control under cycle-based degradation cost," *IEEE Trans. Smart Grid*, vol. 13, no. 6, pp. 4909-4917, Nov. 2022.

[12] S. A. Arefifar, and Y. A. R. I. Mohamed, "DG mix, reactive sources and energy storage units for optimizing microgrid reliability and supply security," *IEEE Trans. Smart Grid*, vol. 5, no. 4, pp. 1835-1844, Jul. 2014.

[13] X. Yan, D. Abbes, and B. Francois, "Uncertainty analysis for day ahead power reserve quantification in an urban microgrid including PV generators," *Renew. Energy*, vol. 106, pp. 288-297, Jun. 2017.

[14] Z. Zhou, Z. Liu, H. Su, and L. Zhang, "Collaborative strategy of dynamic wireless charging electric vehicles and hybrid power system in microgrid," *Int. J. Electr. Power Energy Syst.*, vol. 143, Dec. 2022, Art. no. 108368.

[15] Z. Zhou, Z. Liu, H. Su, and L. Zhang, "Bi-level framework for microgrid capacity planning under dynamic wireless charging of electric vehicles," *Int. J. Electr. Power Energy Syst.*, vol. 141, Oct. 2022, Art. no. 108204.

[16] A. O. Elmeligy, E. ElGhanam, M. S. Hassan, A. H. Osman, A. A. Shalaby, and M. Shaaban, "Optimal planning of dynamic wireless charging infrastructure for electric vehicles," *IEEE Access*, vol. 12, pp. 30661-30673, Jan. 2024.

[17] S. Sraidi, and M. Maaroufi, "Energy management in the microgrid and its optimal planning for supplying wireless charging electric vehicle," *J. Electr. Comput. Eng.*, vol. 2022, Feb. 2022.

[18] P. Mallikarjun, S. Thulasiraman, P. K. Balachandran, and M. Zainuri, "Economic energy optimization in microgrid with PV/wind/battery integrated wireless electric vehicle battery charging system using improved Harris Hawk optimization," *Scientific Reports*, vol. 15, no. 1, Mar. 2025.

[19] B. Li, Z. Liu, and H. Su, "Economic-emission coordinated operation of transportation-microgrid coupled system based on dynamic user equilibrium," *IEEE Trans. Intell. Transp. Syst.*, vol. 26, no. 2, pp. 1–16, Jan. 2024

[20] S. Zhang, X. Zhu, S. Zhang, and J. J. Q. Yu, "Non-cooperative coupled microgrid-transportation coordination system: A deep deterministic policy gradient-based approach," *Int. J. Electr. Power & Energy Syst*., vol. 160, p. 110092, Jul. 2024.

[21] H. Sánchez-Sáinz, C.-A. García-Vázquez, F. Llorens Iborra, and L. M. Fernández-Ramírez, "Methodology for the optimal design of a hybrid charging station of electric and fuel cell vehicles supplied by renewable energies and an energy storage system," *Sustainability*, vol. 11, no. 20, p. 5743, Oct. 2019.

[22] J. Ahmad, M. Tahir, and S. K. Mazumder, "Improved dynamic performance and hierarchical energy management of microgrids with energy routing," *IEEE Trans. Ind. Inform*., vol. 15, no. 6, pp. 3218–3229, Jun. 2019.

[23] X. J. Han, X. Li, and Z. R. Wang, "An optimal control method of microgrid system with household load considering battery service life," *J. Energy Storage*, vol. 56, Dec. 2022, Art. no. 106002.

[24] S. Hu, S. Peeta, C. H. Chu, "Identification of vehicle sensor locations for link-based network traffic applications," *TRANSPORT RES B-METH*, vol. 43, pp. 873-894, Sept. 2009.

[25] W.-L. Jin, *Introduction to network traffic flow theory: principles, concepts, models, and methods*. Cambridge: Elsevier, 2021.

[26] W. H. K. Lam, W. T. Hung, H. K. Lo, H. P. Lo, C. O. Tong, S. C. Wong, and H. Yang, "Advancement of the annual traffic census in Hong Kong," *Proc. Inst. Civ. Eng. Transp*, vol. 156, no. 2, pp. 103–115, May 2003.

[27] M. G. Romana, and D. Hernando, "Obtaining a maximum AADT sustained by two-lane roads: an application to the Madrid region in Spain," *Transp. Res. Proc*, vol. 14, pp. 3209–3217, Jun. 2016.

[28] F. Fang, Z. Zhu, S. Jin, and S. Hu, "Two-layer game theoretic microgrid capacity optimization considering uncertainty of renewable energy," *IEEE Syst. J.*, vol. 15, no. 3, pp. 4260-4271, Sept. 2021.

[29] J. F. Escobedo, E. N. Gomes, A. P. Oliveria, and J. Soares, "Modeling hourly and daily fractions of UV, PAR and NIR to global solar radiation under various sky conditions at Botucatu, Brazil," *Appl. Energy*, vol. 86, no. 3, pp. 299-309, Mar. 2009.

[30] L. Battisti, E. Benini, A. Brighenti, S. D. Anna, and M. R. Castelli, "Small wind turbine effectiveness in the urban environment," *Renew. Energy*, vol. 129, pp. 102-113, Dec. 2018.

[31] S. M. Hakimi, and S. M. Moghaddas-Tafreshi, "Optimal planning of a smart microgrid including demand response and intermittent renewable energy resources," *IEEE Trans. Smart Grid*, vol. 5, no. 6, pp. 2889-2900, Nov. 2014.

[32] S. M. Hosseini, R. Carli and M. Dotoli, "Robust optimal energy management of a residential microgrid under uncertainties on demand and renewable power generation," *IEEE Trans. Autom. Sci. Eng.*, vol. 18, no. 2, pp. 618-637, Apr. 2021.

[33] P. P. Varaiya, F. F. Wu, and J. W. Bialek, "Smart operation of smart grid: risk-limiting dispatch," *Proc. IEEE.*, vol. 99, no. 1, pp. 40-57, Jan. 2011.

[34] M. Zhang, Q. Xu, C. Zhang, L. Nordström, and F. Blaabjerg, "Decentralized coordination and stabilization of hybrid energy storage systems in DC microgrids," *IEEE Trans. Smart Grid*, vol. 13, no. 3, pp. 1751-1761, May 2022.

[35] L. Tziovani, L. Hadjidemetriou, C. Charalampous, M. Tziakouri, S. Timotheou, and E. Kyriakides, "Energy management and control of a flywheel storage system for peak shaving applications," *IEEE Trans. Smart Grid*, vol. 12, no. 5, pp. 4195-4207, Sept. 2021.

[36] S. Córdova, C. Cañizares, Á. Lorca, and D. E. Olivares, "An energy management system with short-term fluctuation reserves and battery degradation for isolated microgrids," *IEEE Trans. Smart Grid*, vol. 12, no. 6, pp. 4668-4680, Nov. 2021.

[37] B. Xu, A. Oudalov, A. Ulbig, G. Andersson, and D. S. Kirschen, "Modeling of lithium-ion battery degradation for cell life assessment," *IEEE Trans. Smart Grid*., vol. 9, no. 2, pp. 1131-1140, Mar. 2018.

[38] Q. Zhang, C. G. Huang, H. Li, G. Feng, and W. Peng, "Electrochemical impedance spectroscopy based state-of-health estimation for lithium-ion battery considering temperature and state-of-charge effect," *IEEE Trans. Transp. Electrif.*, vol. 8, no. 4, pp. 4633-4645, Dec. 2022.

[39] S. K. Han, S. H. Han, and H. Aki, "A practical battery wear model for electric vehicle charging applications," *Appl. Energy*, vol. 113, pp. 1100-1108, Jan. 2014.

[40] J. Lee, and Y. Kim, "Novel battery degradation cost formulation for optimal scheduling of battery energy storage systems," *Int. J. Electr. Power Energy Syst*., vol. 137, May 2022, Art. no. 107795.

[41] CLP Power Hong Kong, "Electricity tariff," 2022. [Online]. Available: www.clp.com.hk/content/dam/clphk/documents/tariff-adjustment-2022/Tariff%20Table%20-%20English%20(2022-01-01).pdf

[42] L. Yan, H. Shen, J. Zhao, C. Xu, F. Luo, C. Qiu, Z. Zhang, and S. Mahmud, "CatCharger: deploying in-motion wireless chargers in a metropolitan road network via categorization and clustering of vehicle traffic," *IEEE Internet Things J.*, vol. 9, no. 12, pp. 9525-9541, Jun. 2022.

[43] Transport Department, "The annual traffic census," 2023. [Online]. Available: atc.td.gov.hk/2022/AnnualTrafficCensus2022.pdf

[44] Y. Tao, J. Qiu, S. Lai, G. Wang, H. Liu, and X. Sun, "Coordinated planning of dynamic wireless charging systems and electricity networks considering range anxiety of electric vehicles," *IEEE Trans. Smart Grid*, vol. 15, no. 4, pp. 3876-3891, Jul. 2024.

[45] S. Nakagawa, and I. C. Cuthill, "Effect size, confidence interval and statistical significance: a practical guide for biologists," *Biological Reviews*, vol. 82, no. 4, pp. 591–605, Nov. 2007.

[46] T. W. MacFarland, *Two-Way Analysis of Variance.* New York: Springer New York, 2012.

[47] X. Zhan, S. V. Ukkusuri, and P. S. C. Rao, "Dynamics of functional failures and recovery in complex road networks," *Physical Rev. E*, vol. 96, no. 5, Nov. 2017, Art. no. 052301.

[48] Beijing Electric Vehicle Co., Ltd. "Charge it." Accessed: Jun. 26, 2025. [Online]. Available: https://www.bjev520.com